Plasma polymer coatings to direct the differentiation of mouse kidney derived stem cells into podocyte-and proximal tubule-like cells

Isabel Hopp[1#], Melanie MacGregor-Ramiasa[2#], Kyle Doherty[3], Rahul M. Visalakshan[2], Krasimir Vasilev[2], Rachel L. Williams[3]* and Patricia Murray[1]

1. Institute of Translational Medicine, University of Liverpool, L69 3GE, UK

2. School of Engineering, Future Industries Institute, University of South Australia, SA 5095, Australia

3. Department of Eye and Vision Science, University of Liverpool, L7 8TX, UK

Joint first author

*corresponding author (rlw@liverpool.ac.uk)

Short running title: **Plasma polymers direct differentiation of kidney-derived stem cells**

Summary

Kidney disease is now recognised as a global health problem and is associated with increased morbidity and mortality, along with high economic costs. To develop new treatments for ameliorating kidney injury and preventing disease progression, there is a need for appropriate renal culture systems for screening novel drugs and investigating the cellular mechanisms underlying renal pathogenesis. There is a need for in vitro culture systems that promote the growth and differentiation of specialised renal cell types. In this work, we have used plasma polymerisation technology to generate gradients of chemical functional groups to explore whether specific concentrations of these functional groups can direct the differentiation of mouse kidney-derived stem cells into specialised renal cell types. We found that amine-rich ($-NH_2$) allylamine-based plasma polymerised coatings could promote differentiation into podocyte-like cells, whereas methyl-rich (CH_3) 1,7-octadiene-based coatings promoted differentiation into proximal tubule-like cell (PTC). Importantly, the PT-like cells generated on the substrates expressed the marker megalin and were able to endocytose albumin, indicating that the cells were functional.

Keywords:

Allylamine, differentiation, kidney disease, megalin, podocyte, proximal tubule cells, renal, stem cells

Introduction

There is an increasing prevalence of chronic kidney disease (CKD) and it has been estimated that 11-13% of the world's population is affected.[1] Most patients with CKD will die of cardiovascular disease[2] and those that survive are likely to progress to end stage kidney disease (ESKD), requiring dialysis or renal transplantation. Currently, understanding the molecular and cellular mechanisms that underlie kidney disease and the development of novel drug therapies is challenging because of the lack of appropriate renal culture systems.[3] The availability of culture systems comprising podocytes and proximal tubule cells (PTC) would be of particular value given that these two cell types are affected in most types of kidney disease.[4-5] Podocytes (visceral epithelial cells) are highly complex cells that form an essential part of the glomerular filtration barrier, whereas PTCs are crucial for the reabsorption of molecules from the urinary filtrate and the excretion of organic anions and cations.[6-7] A problem with culturing these cell types *in vitro* is that podocytes are terminally differentiated cells with no scale-up potential, and PTCs only maintain their functionality and differentiated phenotype for a few days following isolation from the kidney.[8] Although the development of conditionally immortalised podocyte[9] and PTC lines[10] has facilitated progress in this field, the phenotype of such transformed cells does not exactly mimic that of their *in vivo* counterparts.

We have previously isolated a clonal stem cell line from neonatal mouse kidneys and demonstrated that these mouse kidney-derived stem cells (mKSCs) generate podocyte and proximal tubule cells *in vitro* and *ex vivo.*[11-12] Plasma polymerised substrates with varying degrees of nanoroughness and different surface chemistries have shown that substrates comprising a high degree of nanoroughness in combination with high amine content could promote the differentiation into podocyte-like cells (~32% of the mKSC population generating podocytes), whereas surfaces with low amine and high methyl content appeared to promote differentiation towards PTC-like cells, though this was not quantified.[13] Given that the chemical composition of the surfaces appeared to have a greater influence on mKSC differentiation than did the nanotopography, the aim of the current study was to focus specifically on the role of surface group chemistries in regulating the differentiation of mKSCs into podocyte- and PT-like cells. To this end, we generated gradients of plasma polymerised allylamine (AA)- and 1,7-octadiene (OD)-based surfaces to determine the effect of amine- and methyl- rich surfaces without different topographies on mKSC behaviour. The advantage of gradient technology is that it enables rapid identification of the functional group concentration that promotes differentiation to the required cell type. To validate the results obtained with the gradient surfaces, we also assessed mKSC behaviour on the following homogenous plasma polymerised surfaces: (1) 100% OD:0% AA; (2) 75% OD:25% AA; (3) 50% AA :50% OD; (4) 25% OD:75% AA; (5) 0% OD:100% AA.

These homogeneous surfaces will be referred to as 0% AA, 25% AA, 50% AA, 75% AA, and 100% AA, respectively.

Materials and methods

Substrate preparation and sterilisation: Plasma polymerisation was performed in a custom-built 13.56 MHz radiofrequency plasma reactor described previously.[14] 13 mm glass coverslips were cleaned with air plasma for 3 min. Allylamine (AA) (98%, Sigma) and 1,7-octadiene (OD) (98%, Sigma) precursors were mounted on two separate needle valves. The AA:OD ratio entering the plasma polymerisation chamber was carefully controlled by the automated needle valves with a precursor flow rate of 10 sccm. Plasma polymer films were deposited for 30 s at 30 W. Prior to cell culture, substrates were incubated with Penicillin/Streptomycin (Sigma) for 10 min to reduce the risk of infection. Throughout these studies the cultures were examined under the microscope for signs of infection and there was no indication of contamination throughout experiments conducted in these surfaces.

X-ray photoelectron spectroscopy (XPS): The instrument used for this study has been described in detail previously.[15] XPS analyses were conducted using a VSW ESCA XPS spectrometer fitted with an AlKα 1486.6 eV monochromator. Survey, valence, C1s, O1s and N1s spectra were recorded at a 45° take-off angle at 150 eV, 0.8 mm slit, 1.8 kW. Charge compensation was provided by a low energy electron flood gun (Scienta FG300) in the analyses chamber under optimal spectral resolution. The spectra were analysed by curve fitting using CasaXPS (Casa software Ltd) software.

Primary amine quantification: Coomassie Brilliant Blue (CBB): Polymer-coated samples were immersed in 0.3 mL of a solution of 0.5 mg/mL CBB in acidic solution (85:10:5 v/v dH_2O/methanol/acetic acid, pH 2.2) for 5 min at room temperature (RT). To eliminate excess dye, the samples were washed with the acidic solution without dye until the rinsing solution was clear. The samples were then dried at RT in air. To remove the amine-bound dye, 0.3 mL of an alkaline solution (0.125 M K_2CO_3 in 50:50 v/v dH_2O/ methanol, pH 11.25) was added, transferred into a 96 well plate and adjusted to pH 3 (by adding 7.5% v/v of 3 M HCl). The absorbance of the solution was measured at 615 nm. Orange 2: Polymer coated samples were immersed in 0.3 mL of a solution of 14 mg/mL Orange 2 dye in acidic solution (dH_2O at pH 3 adjusted with 1 M HCl) for 30 min at 40°C. To eliminate any excess dye, the samples were thoroughly washed in the acidic solution without dye until the rinsing solution was clear. The samples were then dried at RT in air. To remove the amine-bound dye, 0.3 mL of an alkaline solution (dH_2O at pH 12 adjusted with 1 M NaOH) was added, transferred into a 96 well plate and adjusted to pH 3 (by adding 1% v/v of 12.3 M HCl). The absorbance of the solution was measured at 484 nm. Quantification: Prior measurements a standard

acidic solution of 0.05 g/mL CBB or 0.05 g/mL Orange II was prepared and served as a standard. CBB and Orange 2 were shown to interact with N^+ stoichiometrically 1:1 ($N_{dye} = N_{NH2}$)[16].

Contact angle (CA): Sessile drop and captive bubble CA measurements were conducted using a drop shape analysis system (DSA100m, Krüss) consisting of a piezo dosing head, a camera combined with a microscope and a software controlled micro-step x–y stage. Sessile drop: Droplets of 80 pL degassed and deionized water (dH_2O) were dropped on the substrate and images were recorded. For collection of contact angle maps, the sample stage was moved in x and y directions by 0.5 mm increments and contact angles were collected at each point. Captive bubble: An air bubble of 10 µL in volume was placed on the underside of a sample that was exposed to water using a syringe. The contact angles in degrees were calculated using the circular segment method for both sessile drop and captive bubble measurements.

Protein adsorption study: Protein adsorption onto 100%AA and 100% OD substrates was measured using Micro BCA protein assay kit (Thermo Fisher Scientific, Life Technologies Australia.). 12 well plates (4 cm^2 surface area per well) coated with allylamine and octadiene were used as substrates to study the protein adsorption following established procedures. [17-18] FBS (10%), bovine serum albumin (BSA, Sigma-Aldrich) and fibronectin (GIBCO Invitrogen cell culture , cat no 33016-015), 0.5 mg/mL in phosphate buffer saline (PBS), were pipetted onto the surface and incubated for 1 h at 37 °C. The surface were rinsed three times with PBS to remove the unbound proteins before adding to each well 250 µL of micro BCA reaction solution and incubating for 2 h at 37 °C. The solution were then aspirated and transferred to a 96 well plate for spectrophotometric measurement of the colored solution absorbance at 562 nm. [19] The amount of protein adsorption was calculated from the standard curve. All measurements were conducted in triplicate.

Cell culture and analyses: mKSCs (established by the Stem Cell Research group, University of Liverpool[11-12]) were cultured in DMEM supplemented with 10% FBS, 2mM L-glutamine and 1% MEM non-essential amino acids (Sigma). When cells were cultured on plasma polymerised or control coverslips, the medium was supplemented with 1% penicillin / streptomycin (Sigma) and changed every 2-3 days. Sterile 13 mm plasma coated glass coverslips were transferred to a 24 well plate and cells were seeded at a density of $1x10^3$ cells/well and shaken gently 1 h post seeding to ensure homogeneous distribution of the cells. Cells on coverslips were fixed using 4% (w/v) paraformaldehyde (PFA) and subsequently stained with Alexa Fluor® 488 Phalloidin (Invitrogen) for 30 min at RT (room temperature) in the dark, washed with phosphate buffered saline (PBS) and co-stained with DAPI (Life Technologies) for 15 min at RT, washed and mounted onto microscopy slides and imaged using a Leica DM2500 microscope coupled to a Leica DFC420C camera. An average of 10

fields of view per coverslip were imaged. In order to quantify the number of podocyte-like cells, the proportion of cells with podocyte-like morphology and characteristics was determined under phase contrast [13] from at least 5 fields of view per sample. Briefly, cells displaying characteristic podocytes morphological features including high cytoplasmic-to-nuclear ratio, arborized appearance and binucleation were counted by eye.[12, 20] All experiments were performed in biological triplicates with 3 technical replicates.

Immunofluorescence: Cells were fixed with 4% (w/v) PFA for 5 mins at RT and washed in PBS. The following primary antibodies were used: Mouse anti-megalin (1:200, Acris, DM3613P) and anti-nephrin (1:250, Abcam, ab58968.) The secondary antibodies used were: Alexa fluor-conjugated goat anti-mouse IgG1 (1:500) and Alexa fluor-conjugated chicken anti rabbit IgG (1:500) (all Life Technologies). Primary antibodies were incubated overnight at 4°C; secondary antibodies were incubated for 2h at room temperature. Controls includes samples where the primary antibody was omitted. Nuclei were stained with DAPI. Coverslips were then mounted and images taken using a Leica DM2500 coupled to a Leica DFC420C camera.

Alkaline Phosphatase staining: Following 10 min cell fixation with 4% (w/v) PFA at room temperature cells were washed 3 times with PBS and incubated in Tris-HCl at pH 9.2 for 5 min at room temperature. Subsequently Tris-HCl was removed and cells were incubated in a solution of 2 mg (0.02% (w/v)) naphtol AS-MX phosphate and 10 mg (0.1% (w/v) Fast Red TR in 10 mL Tris-HCl (pH 9.2) for 15 min at room temperature in the dark. The staining solution was then removed and cells were washed once with Tris-HCl pH 9.2 and twice with PBS. Cells were co-stained with DAPI for 30 min in the dark at room temperature. The coverslips were then carefully removed from the 24 well plates and mounted with Dako Fluorescence Mounting Medium and images acquired under epifluorescence illumination using a Leica DM2500 microscope coupled to a Leica DFC420C camera.

Uptake of bovine serum albumin: Cells were cultured in serum free medium for 24 h, then incubated with 40 mg/ml FITC-conjugated bovine serum albumin (F-BSA) (Life Technologies) in serum free medium for 1 h in a humidified chamber with 5% CO_2 at 37 °C. The samples were then washed thoroughly with PBS, trypsinised and analysed using flow cytometry (BD FACScalibur). A minimum of $1x10^4$ cells per coverslip were analysed and the percentage of F-BSA-positive cells was quantified using a BD FACScalibur (BD Biosciences) instrument. Cells cultured on glass were used as controls. All experiments comprised three biological and three technical replicates.

Statistical analyses: One-way analyses of variance (ANOVA) and post-hoc Tukey test were performed to evaluate statistical significances between groups of samples. All statistical analyses were performed using Graphpad (GraphPad Prism v5.0 software for Windows, GraphPad Software Inc.,

San Diego, CA). The statistical significance is shown using the *p*-value (*p*) with $p<0.05$ (*) considered as "significant" $p< 0.01>p>0.001$ (**) "very significant and $p<0.001$ (***) highly significant". If no significant difference was detected this is indicated either in the figure captions or indicated by n.s. (not significant) within the graphs.

Results

Substrate physicochemical analyses

The surface elemental composition was quantified from XPS survey spectra and the nitrogen:carbon (N/C) and oxygen:carbon (O/C) ratios were determined for all homo- and copolymers and across the gradient (**Figure 1A, B**). The results showed that the N/C ratio increased from OD rich surfaces towards AA rich surfaces and this trend was maintained on the gradient substrates, as expected.

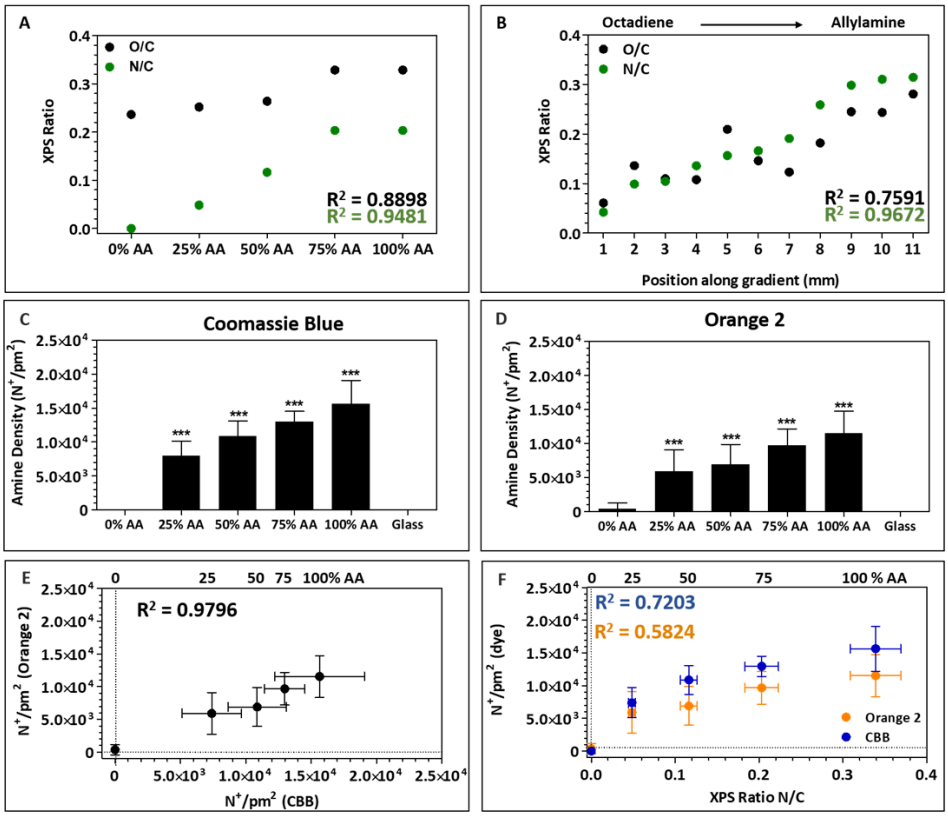

Figure 1: Surface chemical analyses. Oxygen/Carbon (O/C, black) and Nitrogen/Carbon (N/C, green) atomic ratio of (A) homo- and copolymers and (B) across the gradient. (C) Homo-and copolymer surface primary amine quantification using Coomassie Blue (CBB) method and (D) Orange 2 method. (E) Correlation between CBB and Orange 2 method. (F) Correlation between XPS ratio (N/C) and primary amine group density quantification obtained by colorimetry using CBB (blue) and Orange 2 (orange) method. The x-axis error bars correspond to the general XPS 10% error. Data represent an average of a minimum of 5 samples ± SD. Asterisks indicate statistical significance between substrates ($p<0.05$).

Although the surfaces were only composed of carbon and nitrogen, oxygen was detected as a result of surface oxidation due to contact with air, as described previously[21]. Interestingly, substrates with a higher content of AA also showed a higher content of oxygen surface species.

In addition to the analyses of substrate elemental composition, the amount of primary amine groups on the outermost surface of AA and OD homo- and copolymer substrates was quantified via Coomassie Brilliant Blue (CBB) and Orange 2 (**Figure 1C, D**) colorimetric analyses. A maximum of 1.5 x 10^4 ± 0.5 x 10^4 primary amine groups / pm^2 were present on 100% AA coated substrates and this amount decreased with increasing OD content. A 25% increase of OD concentration caused a decrease of about 0.5 x 10^4 primary amine groups / pm^2. This trend was consistent regardless of the dye used. The Orange 2 method showed a small amount of primary amines on the 0% AA samples, but this is likely to be nonspecific binding because the CBB method did not indicate the presence of any amine groups on this substrate. No amines were detected on the glass control substrate. As the amine concentration changed across the gradient substrates, it was not possible to quantify primary amines / pm^2. The results showed a higher amount of primary amines (16.76 ± 1.15 x 10^3) using the CBB method compared to the Orange 2 method (7.86 ± 2.18 x 10^3). A correlation of both methods showed a similar amount of primary amines on the particular substrate (**Figure 1E**); the correlation of the primary amine group density obtained by colorimetry with the amine content obtained from XPS N/C ratio analysis showed an increase in primary amine density with an increasing AA concentration (**Figure 1F**).

Increasing the AA content in the plasma deposited film led to changes in the surface chemistry which were accompanied by changes in wettability, as demonstrated by sessile drop (**Figure 2A-B**) and captive bubble water contact angle measurements (**Figure 2D**). The largest water contact angles were measured on OD rich surfaces (0% AA: ~80 °), whereas increasing AA concentration led to a decrease in the contact angle (100% AA: ~60 °). This trend was confirmed with all measurements across the gradients. However, only small, insignificant ($p>0.05$) differences were obtained on the AA-rich half of the substrate (position 6 mm to 12 mm). The surface wettability analysis was complemented by generating sessile drop water contact angle maps of all surfaces. These maps are used to reveal prominent wettability changes across the surface of the substrate of interest, revealing inconsistencies that could be due to contamination or flaws caused by an uneven distribution of functional groups during the plasma polymerisation process (**Figure 2C**). The distribution of the water contact angles across the surfaces investigated was found to be homogeneous with very little variation. The OD surface was the most hydrophobic (indicated by green colour) and with increasing AA, the surfaces became more hydrophilic (indicated by orange colour). A glass substrate served as a control and was the most hydrophilic substrate. The gradient

substrates showed an even transition (colour change) from the hydrophobic, OD-rich half of the coverslip to the hydrophilic, AA-rich half.

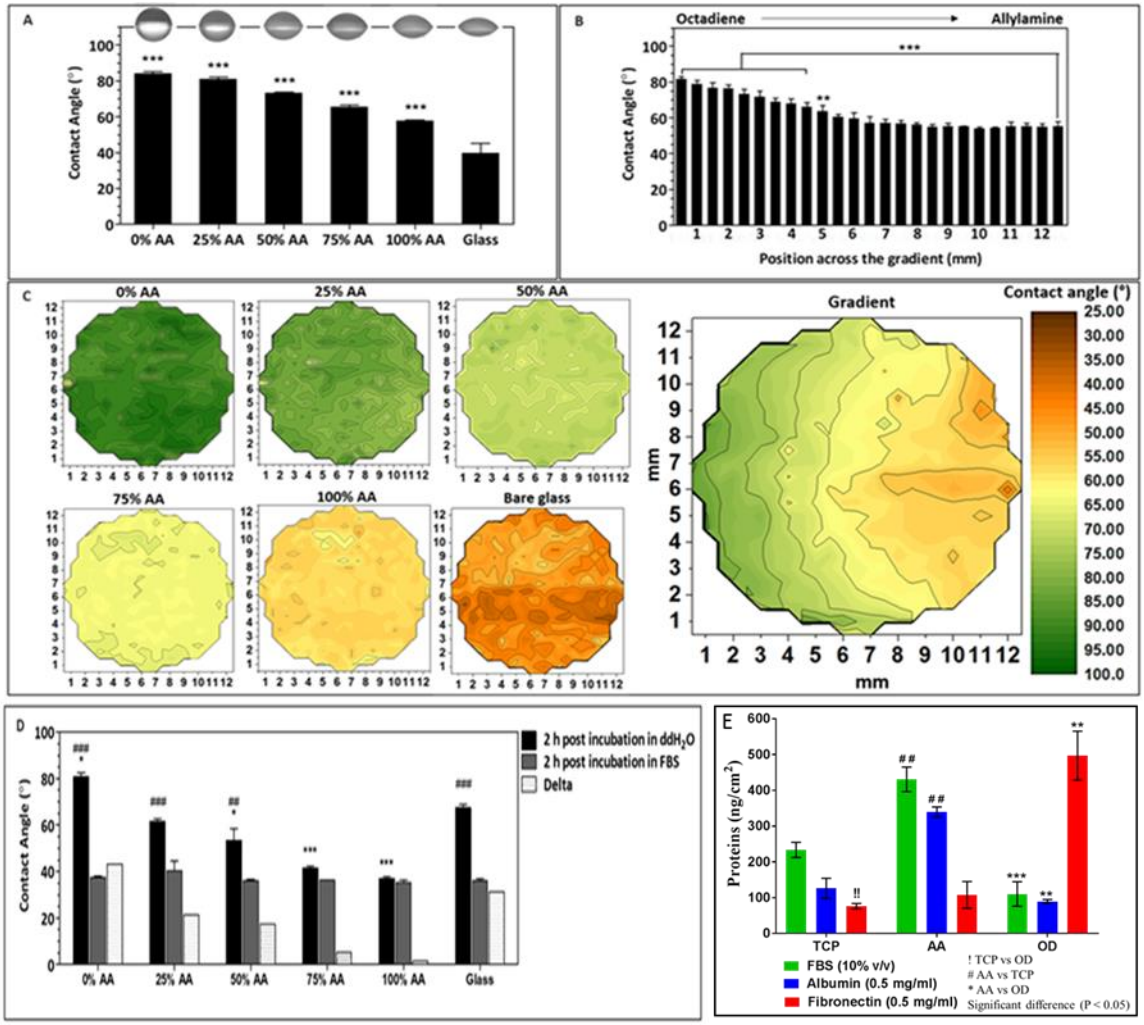

Figure 2: Sessile drop water contact angle of (A) AA and OD homo- and copolymers and (B) across the gradient. Date represent the mean of a minimum of 5 samples ± SD. (C) 2D water contact angle maps, representing the homogeneity of (sessile drop) contact angles across the surface plasma polymer coating. (D) Captive bubble contact angles 2 h post incubation of AA and OD homo- and copolymers in water (ddH_20, black) and FBS (grey). Error bars represent the standard error of a minimum of 5 samples ±SD. Asterisks indicate statistical significance between substrates compared to a glass control (Tukey test, $p < 0.005$). (E) Protein adsorption BCA assay on 100%AA and 100%OD surfaces and tissue culture plate control (TCP) Error bars represent the standard error of a minimum of 5 samples ±SD. "!" symbol indicate statistical difference between TCP and OD, "#" between AA and TCP, "*" between AA and OD ($P < 0.05$)

In addition, the captive bubble method was applied to analyse surface wettability of homo- and copolymers after 2 h incubation in either water (ddH_2O) or foetal bovine serum (FBS) (Figure 2D). In good agreement with the sessile drop measurements described above, OD rich samples were the most hydrophobic surfaces and contact angles decreased significantly with increasing AA

concentration. 2 h post incubation in FBS, the CAs of all substrates were in a very similar range of about 40°.

AFM analyses showed a consistent layer thickness of about 10 ± 5 nm for all substrate and did not reveal any differences in surface roughness (consistently 4 ± 1.5 nm) nor mechanical properties (1 ± 0.3 GPa) (See supplementary information **Figure S1-S4**).

Protein adsorption

In order to further investigate the interaction between the plasma coated surfaces and the cell culture media, protein adsorption assays were conducted in which 100%AA and 100%OD surfaces were incubated with a FBS, albumin or fibronectin solution. The amount of protein adsorbed was consistently higher on the hydrophilic AA coated surfaces than on the tissue culture plate control surface (**Figure 2E**). The OD coated surface bound the least protein from FBS and albumin solutions. Less than 100ng/cm^2 of albumin was measured on OD surface compared to 350ng/cm^2 on AA surfaces. In contrast, significant amounts of fibronectin were bound to the hydrophobic OD surface, in excess of 500ng/cm^2 compared to only 100ng/cm^2 on AA.

Cell response

There was no significant difference in the population doubling times for mKSCs cultured over a 96h period on plasma homo- and copolymer films on any of the substrates (Supplementary **Figure S5**).

Changes in mKSC morphology on the different substrates using phase contrast microscopy and DAPI and phalloidin staining to assess the actin cytoskeleton (**Figure 3A**) after 96h showed a greater proportion of cells on the amine-rich regions of the gradient substrates appeared more spread and had a typical podocyte-like morphology, including a high cytoplasmic-to-nuclear ratio and an arborized cytoskeleton as described previously.[9, 20] In contrast, cells resembling podocytes were rarely seen within mKSC populations cultured on OD-rich sections of the gradients. This trend was confirmed on homo/copolymer substrates (**Figure 3B**).

The number of cells on each substrate that displayed a podocyte-like morphology 96h post seeding was significantly greater when cells were cultured on AA-rich sections of the gradient substrates compared with OD-rich regions and the glass control. This trend was also confirmed on homogeneous copolymer films (**Figure 4A**). This would be consistent with the observation that there appeared to be more podocytes on the AA-rich substrates, as podocyte differentiation is associated with an increase in cell spreading.[12]

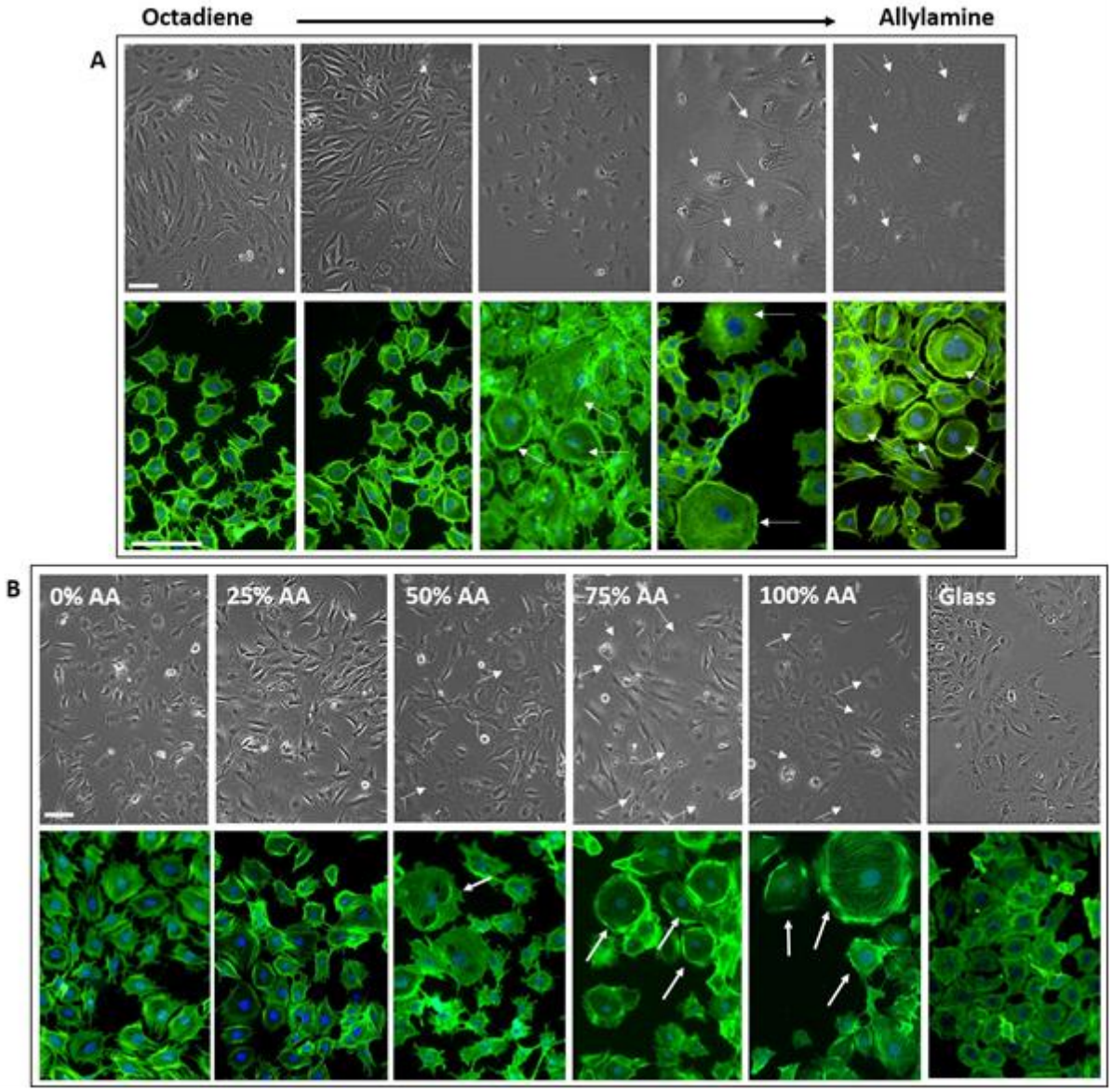

Figure 3: mKSC morphology. Representative phase contrast and phalloidin/DAPI stained fluorescent images of mKSCs cultured on gradients (A) and homo- and copolymers (B) for 96 h. mKSCs were seeded at a density of 1 x 10^3 cells / well. White arrows indicate cells with podocyte-like morphology. Scale bar is 100 µm.

The correlation between cell differentiation into podocyte-like cells and surface amine content (**Figure 4B**) for both homogenous and gradient samples underline our findings (R^2=0.9475, gradient and R^2=0.9303, homogeneous copolymers). To investigate whether these podocyte-like cells also express characteristic markers, these cells were stained for the podocyte specific marker nephrin (NPHS2, **Figure 4C and D**). The images illustrate an increase of podocytes with an increasing concentration of AA. Moreover, many of these cells were binuclear, which is a common characteristic of podocytes in culture (white arrows).

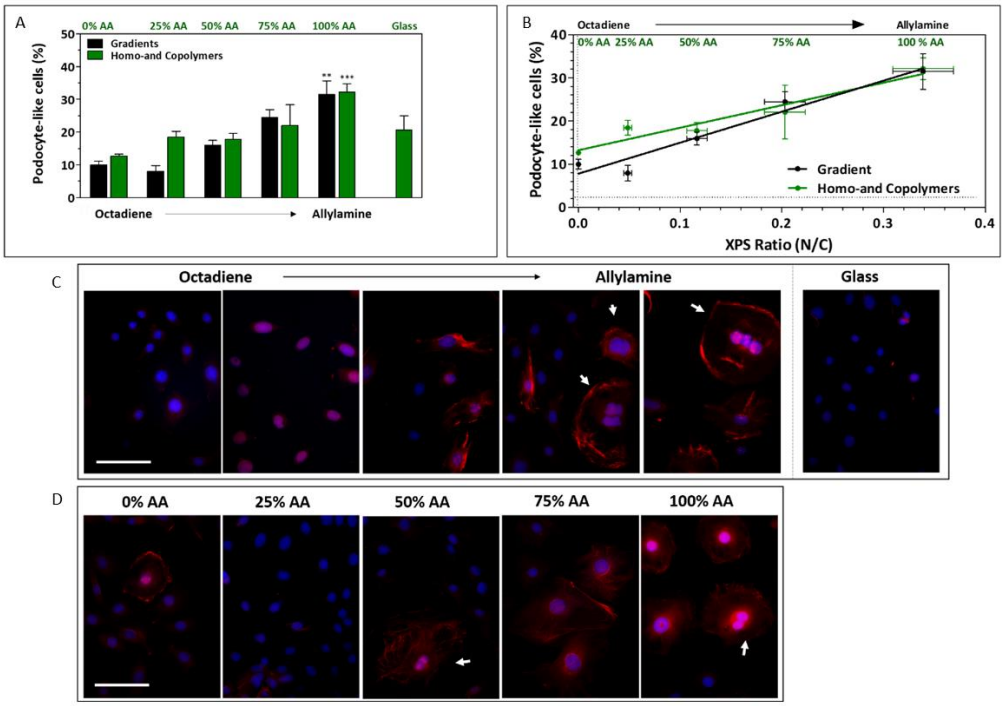

Figure 4: Differentiation of mKSCs into podocyte-like cells. There is a significant increase in the number of podocyte-like cells on amine-rich substrates. mKSCs were seeded at a density of 1 x 10^3 cells / well. (A) Quantification of podocyte-like cells on homo- and copolymers (black bars) and gradients (green bars). (B) Correlation of the amount of podocyte-like cells 96h post seeding with surface amine content as quantified using XPS ratio (N/C) analysis on homo-and copolymers (black) as well as gradients (green), respectively. Asterisks indicate significant differences compared with glass control ($p < 0.05$, Tukey test). Results represent the mean of three biological replicates. (C) Nephrin staining of mKSCs cultured on homo- and copolymers and (D) Nephrin staining of mKSCs cultured on gradients. Blue: DAPI. Red: Nephrin. White arrows indicate binuclear podocyte-like cells. Scale bar: 100 µm.

In order to explore whether plasma polymers also directed mKSC differentiation into proximal tubule (PT)-like cells, mKSCs were stained for the presence of megalin, a PTC transmembrane receptor (**Figure 5A**). The fluorescence micrographs appear to indicate that the number of megalin positive cells (red stain) increased with AA content on the gradient substrates. Results were confirmed on homogeneous films where higher numbers of megalin positive cells were present on OD-rich surfaces compared to AA-rich surfaces and glass controls (**Figure 5B**).

Subsequently the number of megalin expressing cells was quantified at three different time points: 6, 48 and 96h post seeding (**Figure 5C**). The results showed that 6h post seeding, a similar proportion

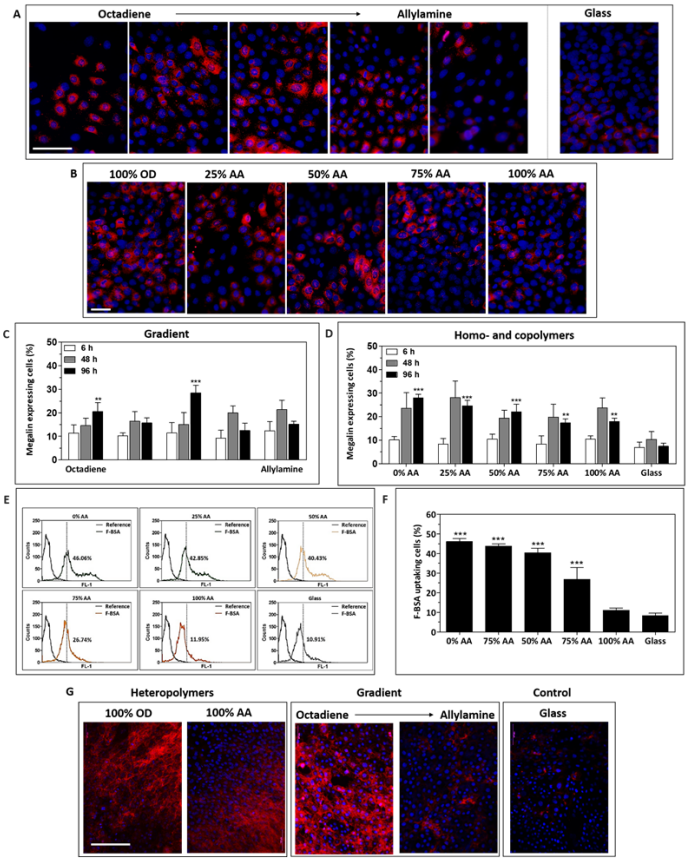

Figure 5: Differentiation of mKSCs into PTCs. There is a significant increase in the number of PTC-like cells on methyl-rich substrates. mKSCs were seeded at a density of 1 x 103 cells / well and cultured for 96 h. (A) Megalin staining of mKSCs cultured on gradient substrates and (B) on homo- and copolymers. Blue: DAPI. Red: megalin. Scale bar: 100 µm (C) Quantification of megalin expressing cells on gradients and (D) homo- and copolymers at three time points, 6 h, 48 h and 96 h post seeding. (E) Flow cytometry data showing F-BSA uptake of cells cultured for 96 h on homo and copolymers. (F) Quantification of F-BSA+ cells cultured on homo- and copolymers. Asterisks indicate significant difference compared to a glass control ($p < 0.05$, Tukey test). Results represent the mean of three biological replicates. (G) Alkaline Phosphatase staining of mKSCs cultured on heteropolymers and AA/OD rich sections of the gradient substrates compared to a glass control. Scale bar: 100 µm

of cells (10%) were megalin positive on all substrates and areas across the gradient which can be attributed to spontaneous differentiation. After 48 and 96h, significantly more megalin positive cells were detected on OD-rich surfaces on homo- and copolymers and gradients (Figure 5C, D). However, on gradient substrates, a greater number of megalin positive cells were also detected towards the middle portion of the substrates. Megalin is a transmembrane receptor that uptakes albumin via endocytosis. Therefore, to investigate whether these PT-like cells displayed this functionality *in vitro,* the cells were cultured for 24 h in serum free medium and subsequently incubated in the presence of fluorescently labelled albumin (F-BSA) for 1h on homo- and copolymers. Our results showed that

the proportion of cells displaying F-BSA uptake was highest on OD rich surfaces (up to ~ 45% of the population). The number of F-BSA up-taking cells decreased with increasing AA concentration **(Figure 5E, F**). It is worth noting that this assay could not be performed on the gradient substrates because it is not feasible to collect enough cells for cytometry analysis from a particular region of the gradient, since it would include cells from adjacent regions and thus distort the results.

Discussion

Substrate physicochemical analyses

The combination of AA and OD in different ratios provides a route to tune the amine surface density.[22-23] In addition, copolymerisation of AA with OD increases AA film stability in aqueous solution, as pure AA films have been shown to quickly undergo ageing, such as surface oxidation.[24] As expected, the XPS analyses showed a high concentration of carbons in all substrates originating from the hydrocarbons within AA and OD films. For both homogeneous and gradient samples, the nitrogen content of the films increased with the AA concentration in the plasma precursor mix. All films also contained oxygen species in increasing proportions as AA concentration increased. This is commonly encountered in plasma polymer films and is typically due to residual moisture in the plasma reactor during polymerisation and post-deposition reaction of the reactive plasma polymer film with oxygen species present in ambient air.[25]

Recent research has shown that the AA plasma layer is composed of several different nitrogen-based chemical groups, including amines, imines, amides and nitrile groups, depending on the experimental conditions.[21, 26] In particular, primary amine group density is expected to increase with AA concentration in the copolymer films.[27] Primary amine groups have been linked to cellular regulation in the past, including enhanced proliferation, adhesion and differentiation.[28-33] Several methods used to quantify primary amine group density have been described previously, including fluorometry and spectrometry, most of which can be very time consuming and expensive.[34-35] Here we employed a colorimetric approach using the two commonly used negatively charged dyes, Coomassie Brilliant Blue (CBB) and Orange 2 that bind to positively charged amine groups via electrostatic interactions.[16, 36] Both dyes showed an increase of primary amine groups with increasing AA concentration, but we observed a higher amount of primary amines when employing the larger CBB molecule compared to the small and monovalent Orange 2. Noel et al. previously used CBB and Orange 2 to quantify the amount of primary amines on aminated polyethylene terephthalate (PET) films and also found that CBB returned higher values than Orange 2,[35] which could possibly result from non-specific adsorption of CBB. Therefore, we conclude that Orange 2 might be more suitable for primary amine quantification.

Both sessile drop and captive bubble contact angle measurements showed a decreasing contact angle with increasing AA concentration. This is due to the fact that AA contains a large number of nitrogen functional groups, prone to hydrogen bonding,[27, 33, 37] as well as oxygen species. The captive bubble method allowed the surface analyses of substrates in a more physiological relevant environment. For instance, AA films are composed of a complex and flexible network that can rearrange itself to minimise the interfacial energy.[38] Thus, in an aqueous environment it is more likely that the hydrophilic groups will align at the surface, contributing to the increased wettability of AA rich films. After exposure to FBS, all contact angles decreased and were more comparable to each other, irrespective of the AA content. This suggests protein adsorption increases the wettability of the hydrophobic surfaces even though we demonstrated that more FBS adsorbed to the AA than the OD surfaces. This phenomenon is known to occur within seconds due to a cumulative effect of non-covalent interactions, such as electrostatic interactions and van der Waals forces.[39-40] The contact angles on the hydrophilic surfaces did not reveal any significant differences between the substrates pre- or post-exposure to FBS.[41-42]

We also found that the chemical substrate composition did not affect surface topography and mechanical properties. Therefore, the results suggested a rather smooth surface and transition from the hydrocarbon rich side to the AA rich side of the gradient without the formation of distinct surface structures.

Mouse KSC behaviour

We found that the population doubling time for the mKSCs was similar on all plasma films, indicating that changes in surface chemistry did not significantly influence mKSC proliferation. We found, however, that mKSCs showed a significantly greater propensity to differentiate into podocyte-like cells on AA-rich surfaces, and into PT-like cells on OD-rich surfaces. This was initially identified using the gradient surfaces and then confirmed using the homogeneous surfaces, demonstrating that the gradient technology can be a convenient approach for rapidly identifying the optimal surface chemistry required for directing the differentiation of stem cells into particular types of specialised cells.

At this stage the mechanisms by which surface functional groups stimulate mKSC differentiation into podocyte- and PT-like cells remain unclear. However, several groups have shown enhanced cell adhesion and the promotion of cellular differentiation on hydrophilic surfaces,[43-44] introduced by a high amine content and potentially oxygen species that were introduced during exposure of substrates to air. For example, adipose derived stromal cells spread more on positively charged amine groups and neutral hydroxyl groups, whereas they displayed a smaller phenotype and

differentiated towards adipocytes on -CH_3 functional groups.[45] These studies correlate with the present study in that, AA rich, hydrophilic surfaces showed an increased number of cells with a more spread podocyte-like morphology, whereas cells on the more hydrophobic, carbon rich substrates had a more typical mKSC phenotype and did not spread as much. We speculate that surface amine groups, which are positively charged under cell culture conditions and generally confer amine-rich plasma coated substrates their cytocompatibility,[46-47] may induce changes in morphology, which may in turn induce cellular mKSC differentiation into podocyte-like cells. Moreover, also the adsorption of proteins from the medium and added serum onto the substrates might have impacted on the cell differentiation.[48] We demonstrated that the amount of FBS, albumin and fibronectin were different on the different surfaces with more fibronectin bound to the OD than the AA surfaces and more albumin and FBS bound to the AA than the OD surfaces and this may hint that the composition of the adsorbed protein layer changes along the gradient of wettability . The two major proteins in serum are albumin and globulin. With an isoelectric point (pI) of 4.7 and molecular weight of 66.5 kDa, BSA has been reported to adhere in larger quantities and with higher adhesion strength to hydrophilic than to hydrophobic surfaces.[49] It is commonly used to limit cell attachment and block non-specific binding. Fibronectin is also present in serum, but in smaller concentration and unlike albumin, Fn has been shown to enhance integrin-receptor-based cell adhesion and spreading while reducing cell migration. With a pI of 5.6, fibronectin is constituted of two 220KDa subunit, both containing several Arg-Gly-Asp (RGD) domains which act as cell binding region.[50] The presence of surface functional groups can influence the conformation of the adsorbed proteins and therefore cell attachment, differentiation and also migration.[45, 51-53] It is more likely that there will be changes in the conformation of proteins adsorbed onto more hydrophobic surfaces (OD) than hydrophilic surfaces (AA). This could lead to the characteristics of the protein layer being different across the gradients and thus influence the differentiation of the mKSC.

Using substrates with density gradient nanotopographical features, we have recently shown that podocyte differentiation is enhanced on rougher surfaces with high nanofeature density, especially when coated with AA-rich plasma-polymerised films, where the proportion of podocyte-like cells reached 30-35% of the population.[13] In the current study we found that on AA-rich surfaces, the proportion of podocytes-like cells reached 30-35% of the mKSC population, despite the fact that these surfaces were relatively smooth suggesting that surface chemistry has a greater influence on differentiation of mKSC to podocyte-like cells than does nanoroughness.

Our previous work also showed that differentiation into PT-like cells was independent of surface topography and appeared to be enhanced on OD-rich surfaces, although this was not quantified. In the current study, we found that following culture on the gradient surfaces, the proportion of cells

expressing the megalin was maximal at the mid-point of the gradient (~50% OD), where ~30% of the population expressed megalin. Interestingly, on the homogeneous surfaces, the proportion of megalin-expressing cells was maximal on the 100% OD surfaces (~30% of the population expressing megalin). We hypothesise that this disparity could be due to the fact that on the gradient substrates, there would be a higher proportion of podocyte-like cells on the AA-rich part of the gradient due to the characteristics of the protein layer adsorbed to that part of the gradient. In the developing kidney, podocytes within the nascent glomeruli express BMP7, which stimulates PTC proliferation in the adjacent tubules.[54] It is therefore possible that PT-like cells present at the mid-point of the gradient might have been exposed to higher levels of BMP7 than those at the OD-rich part of the gradient, leading to enhanced proliferation.

In this study we have shown the importance of surface functional groups on the differentiation of mKSCs and we have shown that AA-rich substrates promote the differentiation into podocyte-like cells and OD-rich surfaces into PT-like cells. Surface chemistry acts as an important cue that highly influences cell behaviour through the characteristics of the adsorbed protein layer. Although the exact mechanisms still remain unclear, it is often correlated with a release of signalling molecules, such as growth factors or glycoproteins, through cell adsorption.[55] For example, Benoit et al. investigated the effects of small molecules on mesenchymal stem cell (MSC) differentiation on 2D arrays and found that phosphate groups (physiological important for bone mineralisation) directed cell differentiation into osteocytes, whereas carboxyl groups (mimic GAGs in cartilage) directed cell differentiation into chondrocytes and *t*-butyl groups (mimic lipid sustained environment) into adipocytes.[56]

A number of recent studies have highlighted the importance of surface nano- and microscale structures, chemistry and elasticity of the extracellular matrix (ECM) in regulating cell behaviour, including morphology, differentiation or migration [57-61] and this has led to an increased development of natural biomaterials that are based on ECM proteins.[58, 62-65] Cellular differentiation is a highly controlled process and micro environmental interactions, such as soluble signals, are critical to support or even initiate this process. A major drawback of natural biomaterials is the difficulty to manipulate their physical and chemical cues, whereas synthetic biomaterials can be designed and tuned in order to mimic these properties. As an alternative, developing synthetic substrates to induce this process provides a simple and inexpensive tool to evaluate such complex processes, as these can provide often simple chemical and physical cues to induce differentiation triggering effects and have been proven to be helpful tools in assessing cellular behaviours.[22, 56, 66] The interactions at the cell-substrate interface is a complex microenvironment in which the material surface can influence cell behaviour through its physical and chemical properties via the adsorbed proteins. The

cell response can also result in remodelling the surface and lead to a change in their behaviour, such as cytoskeletal organisation and differentiation.[56, 67-77] Defining the substrate properties which drive cell differentiation to a specific phenotype could provide a route to the production of in vitro cell culture systems to study the molecular and cellular mechanisms that underlie specific diseases and the development of novel drug therapies.

Conclusions

This study has demonstrated that plasma polymerisation technology can generate gradients of chemical functional groups and that specific concentrations of these functional groups can direct the differentiation of mouse kidney-derived stem cells into specialised renal cell types. We found that amine-rich ($-NH_2$) allylamine-based plasma polymerised coatings could promote differentiation into podocyte-like cells, whereas methyl-rich (CH_3) 1,7-octadiene-based coatings promoted differentiation into proximal tubule-like cell (PTC). Importantly, the PT-like cells generated on the substrates expressed the marker megalin and were able to endocytose albumin, indicating that the cells were functional. This is important in the design of defined in vitro cell culture systems for disease modelling.

Acknowledgements

The authors gratefully acknowledge funding support from the FP7 NephroTools ITN (289754) and Alder Hey Children's Kidney Fund. We also wish to acknowledge Paul Unsworth (University of Liverpool) for the collection of XPS spectra. The authors are grateful to School of Engineering (University of Liverpool) for access to the AFM, and to Drs Tim Joyce and Riaz Akhtar for providing technical assistance.

Conflicts of interest

None of the authors have any conflicts of interest

References

1. Hill, N. R.; Fatoba, S. T.; Oke, J. L.; Hirst, J. A.; O'Callaghan, C. A.; Lasserson, D. S.; Hobbs, F. D. R., Global Prevalence of Chronic Kidney Disease – A Systematic Review and Meta-Analysis. *PLoS ONE* **2016,** *11* (7), e0158765. DOI: https://doi.org/10.1371/journal.pone.0158765.
2. Alani, H.; Tamimi, A.; Tamimi, N., Cardiovascular co-morbidity in chronic kidney disease: Current knowledge and future research needs. *World J Nephrol* **2014,** *3* (4), 156-68. DOI: https://doi.org/10.5527/wjn.v3.i4.156.
3. Murray, P.; Vasilev, K.; Fuente Mora, C.; Ranghini, E.; Tensaout, H.; Rak-Raszewska, A.; Wilm, B.; Edgar, D.; Short, R. D.; Kenny, S. E., The potential of small chemical functional groups for directing

the differentiation of kidney stem cells. *Biochem. Soc. Trans.* **2010,** *38* (4), 1062-6. DOI: https://doi.org/10.1042/BST0381062.
4. Yoo, T.; Li, J.; Kim, J.; Jung, D.; Kwak, S.; Ryu, D.; Choi, H.; Kim, J.; Kim, H.; Han, S., Activation of the renin–angiotensin system within podocytes in diabetes. *Kidney Int.* **2007,** *71* (10), 1019-1027. DOI: https://doi.org/10.1038/sj.ki.5002195.
5. Magri, C. J.; Fava, S., The role of tubular injury in diabetic nephropathy. *Eur. J. Intern. Med.* **2009,** *20* (6), 551-555. DOI: https://doi.org/10.1016/j.ejim.2008.12.012.
6. Hermann, P.; Henry, G.; Wilhelm, K.; Cristina, M.; Matthias, K.; Monique, B., Cell Biology of the Glomerular Podocyte. *Physiol. Rev.* **2003,** *83* (1), 253-261. DOI: https://doi.org/10.1152/physrev.00020.2002.
7. Grgic, I.; Campanholle, G.; Bijol, V.; Wang, C.; Sabbisetti, V. S.; Ichimura, T.; Humphreys, B. D.; Bonventre, J. V., Targeted proximal tubule injury triggers interstitial fibrosis and glomerulosclerosis. *Kidney Int.* **2012,** *82* (2), 172-83. DOI: https://doi.org/10.1038/ki.2012.20.
8. Terryn, S.; Jouret, F.; Vandenabeele, F.; Smolders, I.; Moreels, M.; Devuyst, O.; Steels, P.; Kerkhove, E. V., A primary culture of mouse proximal tubular cells, established on collagen-coated membranes. *American Journal of Physiology - Renal Physiology* **2007,** *293* (2), F476-F485. DOI: https://doi.org/10.1152/ajprenal.00363.2006.
9. Saleem, M. A.; O'Hare, M. J.; Reiser, J.; Coward, R. J.; Inward, C. D.; Farren, T.; Xing, C. Y.; Ni, L.; Mathieson, P. W.; Mundel, P., A conditionally immortalized human podocyte cell line demonstrating nephrin and podocin expression. *Journal of the American Society of Nephrology* **2002,** *13* (3), 630-8.
10. Wilmer, M. J.; Saleem, M. A.; Masereeuw, R.; Ni, L.; van der Velden, T. J.; Russel, F. G.; Mathieson, P. W.; Monnens, L. A.; van den Heuvel, L. P.; Levtchenko, E. N., Novel conditionally immortalized human proximal tubule cell line expressing functional influx and efflux transporters. *Cell Tissue Res.* **2010,** *339* (2), 449-457. DOI: https://doi.org/10.1007/s00441-009-0882-y.
11. Fuente-Mora, C., Isolation and characterisation of a novel population of potential kidney stem cells from postnatal mouse kidney. *School of Biomedical Science, University of Liverpool, PhD-Thesis* **2009**.
12. Ranghini, E.; Mora, C. F.; Edgar, D.; Kenny, S. E.; Murray, P.; Wilm, B., Stem cells derived from neonatal mouse kidney generate functional proximal tubule-like cells and integrate into developing nephrons *in vitro*. *PLoS ONE* **2013,** *8* (5), e62953. DOI: https://doi.org/10.1371/journal.pone.0062953.
13. MacGregor-Ramiasa, M.; Hopp, I.; Bachhuka, A.; Murray, P.; Vasilev, K., Surface nanotopography guides kidney-derived stem cell differentiation into podocytes. *Acta Biomater.* **2017,** *56*, 171-180. DOI: https://doi.org/10.1016/j.actbio.2017.02.036.
14. Griesser, H. J., Small scale reactor for plasma processing of moving substrate web. *Vacuum* **1989,** *39* (5), 485-488. DOI: http://dx.doi.org/10.1016/0042-207X(89)90272-8.
15. Weightman, P., A new high sensitivity Auger spectrometer. *Phys. Scr.* **1992,** *T41*, 277-281. DOI: https://doi.org/10.1088/0031-8949/1992/T41/050.
16. Coussot, G.; Nicol, E.; Commeyras, A.; Desvignes, I.; Pascal, R.; Vandenabeele-Trambouze, O., Colorimetric quantification of amino groups in linear and dendritic structures. *Polym. Int.* **2009,** *58* (5), 511-518. DOI: https://doi.org/10.1002/pi.2560.
17. Nomura, K.; Mikuni, S.; Nakaji-Hirabayashi, T.; Gemmei-Ide, M.; Kitano, H.; Noguchi, H.; Uosaki, K., Water structure at the interfaces between a zwitterionic self-assembled monolayer/liquid water evaluated by sum-frequency generation spectroscopy. *Colloids and Surfaces B: Biointerfaces* **2015,** *135*, 267-273. DOI: http://dx.doi.org/10.1016/j.colsurfb.2015.07.072.
18. Nomura, K.; Nakaji-Hirabayashi, T.; Gemmei-Ide, M.; Kitano, H.; Noguchi, H.; Uosaki, K., Sum-frequency generation analyses of the structure of water at amphoteric SAM–liquid water interfaces. *Colloids and Surfaces B: Biointerfaces* **2014,** *121*, 264-269. DOI: http://dx.doi.org/10.1016/j.colsurfb.2014.04.025.

19. Hung, A.; Mwenifumbo, S.; Mager, M.; Kuna, J. J.; Stellacci, F.; Yarovsky, I.; Stevens, M. M., Ordering surfaces on the nanoscale: implications for protein adsorption. *J. Am. Chem. Soc.* **2011,** *133* (5), 1438-1450. DOI: https://doi.org/10.1021/ja108285u.
20. Fuente Mora, C.; Ranghini, E.; Bruno, S.; Bussolati, B.; Camussi, G.; Wilm, B.; Edgar, D.; Kenny, S. E.; Murray, P., Differentiation of podocyte and proximal tubule-like cells from a mouse kidney-derived stem cell line. *Stem Cells Dev.* **2012,** *21* (2), 296-307. DOI: https://doi.org/10.1089/scd.2010.0470.
21. Choukourov, A.; Biederman, H.; Slavinska, D.; Hanley, L.; Grinevich, A.; Boldyryeva, H.; Mackova, A., Mechanistic studies of plasma polymerization of allylamine. *The Journal of Physical Chemistry B* **2005,** *109* (48), 23086-23095. DOI: https://doi.org/10.1021/jp0535691.
22. Beck, A. J.; Jones, F. R.; Short, R. D., Plasma copolymerization as a route to the fabrication of new surfaces with controlled amounts of specific chemical functionality. *Polymer* **1996,** *37* (24), 5537-5539. DOI: https://doi.org/10.1016/S0032-3861(96)00479-X.
23. Vasilev, K.; Mierczynska, A.; Hook, A. L.; Chan, J.; Voelcker, N. H.; Short, R. D., Creating gradients of two proteins by differential passive adsorption onto a PEG-density gradient. *Biomaterials* **2010,** *31* (3), 392-397. DOI: https://doi.org/10.1016/j.biomaterials.2009.09.056.
24. Tarasova, A.; Hamilton-Brown, P.; Gengenbach, T.; Griesser, H. J.; Meagher, L., Colloid probe AFM and XPS study of time-dependent aging of amine plasma polymer coatings in aqueous media. *Plasma Process. Polym.* **2008,** *5* (2), 175-185. DOI: https://doi.org/10.1002/ppap.200700054s.
25. Whittle, J. D.; Short, R. D.; Douglas, C.; Davies, J., Differences in the aging of allyl alcohol, acrylic acid, allylamine, and octa-1, 7-diene plasma polymers as studied by X-ray photoelectron spectroscopy. *Chem. Mater.* **2000,** *12* (9), 2664-2671. DOI: https://doi.org/10.1021/cm0002158.
26. Krishnamurthy, V.; Kamel, I. L.; Wei, Y., Analysis of plasma polymerization of allylamine by FTIR. *J. Polym. Sci., Part A: Polym. Chem.* **1989,** *27* (4), 1211-1224. DOI: https://doi.org/10.1002/pola.1989.080270409.
27. Goreham, R. V.; Short, R. D.; Vasilev, K., Method for the generation of surface-bound nanoparticle density gradients. *The Journal of Physical Chemistry C* **2011,** *115* (8), 3429-3433. DOI: https://doi.org/10.1021/jp111221g.
28. Tatoulian, M.; Brétagnol, F.; Arefi-Khonsari, F.; Amouroux, J.; Bouloussa, O.; Rondelez, F.; Paul, A. J.; Mitchell, R., Plasma deposition of allylamine on polymer powders in a fluidized bed reactor. *Plasma Process. Polym.* **2005,** *2* (1), 38-44. DOI: https://doi.org/10.1002/ppap.200400029.
29. Fally, F.; Doneux, C.; Riga, J.; Verbist, J., Quantification of the functional groups present at the surface of plasma polymers deposited from propylamine, allylamine, and propargylamine. *J. Appl. Polym. Sci.* **1995,** *56* (5), 597-614. DOI: https://doi.org/10.1002/app.1995.070560509.
30. Myung, S. W.; Choi, H. S., Chemical structure and surface morphology of plasma polymerized-allylamine film. *Korean J. Chem. Eng.* **2006,** *23* (3), 505-511. DOI: https://doi.org/10.1007/BF02706757.
31. Siow, K. S.; Britcher, L.; Kumar, S.; Griesser, H. J., Plasma methods for the generation of chemically reactive surfaces for biomolecule immobilization and cell colonization-A Review. *Plasma Process. Polym.* **2006,** *3* (6-7), 392-418. DOI: https://doi.org/10.1002/ppap.200600021.
32. Mwale, F.; Girard-Lauriault, P.-L.; Wang, H. T.; Lerouge, S.; Antoniou, J.; Wertheimer, M. R., Suppression of genes related to hypertrophy and osteogenesis in committed human mesenchymal stem cells cultured on novel nitrogen-rich plasma polymer coatings. *Tissue Eng.* **2006,** *12* (9), 2639-2647. DOI: https://doi.org/10.1089/ten.2006.12.2639.
33. Truica-Marasescu, F.; Wertheimer, M. R., Nitrogen-rich plasma-polymer films for biomedical applications. *Plasma Process. Polym.* **2008,** *5* (1), 44-57. DOI: https://doi.org/10.1002/ppap.200700077.
34. Janolino, V. G.; Swaisgood, H. E., A spectrophotometric assay for solid phase primary amino groups. *Appl. Biochem. Biotechnol.* **1992,** *36* (2), 81-85. DOI: https://doi.org/10.1007/BF02929687.
35. Aflori, M.; Drobota, M.; Timpu, D.; Barboiu, V., Studies of amine treatments influence on poly (ethyleneterepthalate) films. *Optoelectron. Adv. Mater., Rapid Commun.* **2008,** *2* (5), 291-295.

36. Albrecht, W.; Seifert, B.; Weigel, T.; Schossig, M.; Holländer, A.; Groth, T.; Hilke, R., Amination of poly (ether imide) membranes using di-and multivalent amines. *Macromol. Chem. Phys.* **2003,** *204* (3), 510-521. DOI: https://doi.org/10.1002/macp.200390016.
37. Girard-Lauriault, P.-L.; Mwale, F.; Iordanova, M.; Demers, C.; Desjardins, P.; Wertheimer, M. R., Atmospheric Pressure Deposition of Micropatterned Nitrogen-Rich Plasma-Polymer Films for Tissue Engineering. *Plasma Process. Polym.* **2005,** *2* (3), 263-270. DOI: https://doi.org/10.1002/ppap.200400092.
38. Gengenbach, T. R.; Vasic, Z. R.; Li, S.; Chatelier, R. C.; Griesser, H. J., Contributions of restructuring and oxidation to the aging of the surface of plasma polymers containing heteroatoms. *Plasmas and Polymers* **1997,** *2* (2), 91-114. DOI: https://doi.org/10.1007/BF02766026.
39. Norde, W., Adsorption of proteins from solution at the solid-liquid interface. *Adv. Colloid Interface Sci.* **1986,** *25*, 267-340. DOI: https://doi.org/10.1016/0001-8686(86)80012-4.
40. Wilson, C. J.; Clegg, R. E.; Leavesley, D. I.; Pearcy, M. J., Mediation of biomaterial-cell interactions by adsorbed proteins: a review. *Tissue Eng.* **2005,** *11* (1-2), 1-18. DOI: https://doi.org/10.1089/ten.2005.11.1.
41. Vogler, E. A., Structure and reactivity of water at biomaterial surfaces. *Adv. Colloid Interface Sci.* **1998,** *74* (1–3), 69-117. DOI: http://dx.doi.org/10.1016/S0001-8686(97)00040-7.
42. Absolom, D.; Zingg, W.; Neumann, A., Protein adsorption to polymer particles: role of surface properties. *J. Biomed. Mater. Res.* **1987,** *21* (2), 161-171. DOI: https://doi.org/10.1002/jbm.820210202.
43. Groth, T.; Altankov, G., Cell-surface interactions and the tissue compatibility of biomedical materials. In *New Biomedical Materials: Basic and Applied Studies*, Haris, P. I.; Chapman, D., Eds. ISO Press: Amsterdam, Netherlands, 1998; pp 12-23.
44. Satriano, C.; Conte, E.; Marletta, G., Surface chemical structure and cell adhesion onto ion beam modified polysiloxane. *Langmuir* **2001,** *17* (7), 2243-2250. DOI: https://doi.org/10.1021/la001321r.
45. Chieh, H.-F.; Su, F.-C.; Lin, S.-C.; Shen, M.-R.; Liao, J.-D., Migration patterns and cell functions of adipose-derived stromal cells on self-assembled monolayers with different functional groups. *J. Biomater. Sci. Polym. Ed.* **2013,** *24* (1), 94-117. DOI: https://doi.org/10.1163/156856212X626208.
46. Liu, X.; Feng, Q.; Bachhuka, A.; Vasilev, K., Surface modification by allylamine plasma polymerization promotes osteogenic differentiation of human adipose-derived stem cells. *ACS Applied Materials and Interfaces* **2014,** *6* (12), 9733-9741. DOI: https://www.doi.org/10.1021/am502170s.
47. Liu, X.; Shi, S.; Feng, Q.; Bachhuka, A.; He, W.; Huang, Q.; Zhang, R.; Yang, X.; Vasilev, K., Surface chemical gradient affects the differentiation of human adipose-derived stem cells via ERK1/2 signaling pathway. *ACS Applied Materials and Interfaces* **2015,** *7* (33), 18473-18482. DOI: https://doi.org/10.1021/acsami.5b04635.
48. Webb, K.; Hlady, V.; Tresco, P. A., Relative importance of surface wettability and charged functional groups on NIH 3T3 fibroblast attachment, spreading, and cytoskeletal organization. *J. Biomed. Mater. Res.* **1998,** *41* (3), 422-430. DOI: https://doi.org/10.1002/(SICI)1097-4636(19980905)41:3<422::AID-JBM12>3.0.CO;2-K.
49. Jeyachandran, Y. L.; Mielczarski, E.; Rai, B.; Mielczarski, J. A., Quantitative and qualitative evaluation of adsorption/desorption of bovine serum albumin on hydrophilic and hydrophobic surfaces. *Langmuir* **2009,** *25* (19), 11614-20. DOI: https://doi.org/10.1021/la901453a.
50. Vadillo-Rodriguez, V.; Pacha-Olivenza, M. A.; Gonzalez-Martin, M. L.; Bruque, J. M.; Gallardo-Moreno, A. M., Adsorption behavior of human plasma fibronectin on hydrophobic and hydrophilic Ti6Al4V substrata and its influence on bacterial adhesion and detachment. *J. Biomed. Mater. Res. A* **2013,** *101* (5), 1397-404. DOI: https://doi.org/10.1002/jbm.a.34447.
51. Arima, Y.; Iwata, H., Effect of wettability and surface functional groups on protein adsorption and cell adhesion using well-defined mixed self-assembled monolayers. *Biomaterials* **2007,** *28* (20), 3074-3082. DOI: https://doi.org/10.1016/j.biomaterials.2007.03.013.

52. García, A. J.; Vega, M. a. D.; Boettiger, D., Modulation of Cell Proliferation and Differentiation through Substrate-dependent Changes in Fibronectin Conformation. *Mol. Biol. Cell* **1999,** *10* (3), 785-798. DOI: https://doi.org/10.1091/mbc.10.3.785.
53. Shelton, R.; Rasmussen, A.; Davies, J., Protein adsorption at the interface between charged polymer substrata and migrating osteoblasts. *Biomaterials* **1988,** *9* (1), 24-29. DOI: https://doi.org/10.1016/0142-9612(88)90065-8.
54. Kazama, I.; Mahoney, Z.; Miner, J. H.; Graf, D.; Economides, A. N.; Kreidberg, J. A., Podocyte-derived BMP7 is critical for nephron development. *Journal of the American Society of Nephrology* **2008,** *19* (11), 2181-2191. DOI: https://doi.org/10.1681/ASN.2007111212.
55. Gandavarapu, N. R.; Mariner, P. D.; Schwartz, M. P.; Anseth, K. S., Extracellular matrix protein adsorption to phosphate-functionalized gels from serum promotes osteogenic differentiation of human mesenchymal stem cells. *Acta Biomater.* **2013,** *9* (1), 4525-4534. DOI: https://doi.org/10.1016/j.actbio.2012.09.007.
56. Benoit, D. S. W.; Schwartz, M. P.; Durney, A. R.; Anseth, K. S., Small functional groups for controlled differentiation of hydrogel-encapsulated human mesenchymal stem cells. *Nat. Mater.* **2008,** *7* (10), 816-823. DOI: https://doi.org/10.1038/nmat2269.
57. Gittens, R. A.; McLachlan, T.; Olivares-Navarrete, R.; Cai, Y.; Berner, S.; Tannenbaum, R.; Schwartz, Z.; Sandhage, K. H.; Boyan, B. D., The effects of combined micron-/submicron-scale surface roughness and nanoscale features on cell proliferation and differentiation. *Biomaterials* **2011,** *32* (13), 3395-3403. DOI: https://doi.org/10.1016/j.biomaterials.2011.01.029.
58. Romano, N. H.; Sengupta, D.; Chung, C.; Heilshorn, S. C., Protein-engineered biomaterials: nanoscale mimics of the extracellular matrix. *Biochimica et Biophysica Acta (BBA)-General Subjects* **2011,** *1810* (3), 339-349. DOI: https://doi.org/10.1016/j.bbagen.2010.07.005.
59. Engler, A. J.; Sen, S.; Sweeney, H. L.; Discher, D. E., Matrix Elasticity Directs Stem Cell Lineage Specification. *Cell* **2006,** *126* (4), 677-689. DOI: https://doi.org/10.1016/j.cell.2006.06.044.
60. Discher, D. E.; Janmey, P.; Wang, Y., Tissue cells feel and respond to the stiffness of their substrate. *Science* **2005,** *310* (5751), 1139-1143. DOI: https://doi.org/10.1126/science.1116995.
61. Gobin, A. S.; West, J. L., Cell migration through defined, synthetic ECM analogs. *The FASEB journal* **2002,** *16* (7), 751-753. DOI: https://doi.org/10.1096/fj.01-0759fje.
62. Kalaskar, D. M.; Downes, J. E.; Murray, P.; Edgar, D. H.; Williams, R. L., Characterization of the interface between adsorbed fibronectin and human embryonic stem cells. *Journal of The Royal Society Interface* **2013,** *10* (83), 20130139. DOI: https://doi.org/10.1098/rsif.2013.0139.
63. Koenig, A. L.; Gambillara, V.; Grainger, D. W., Correlating fibronectin adsorption with endothelial cell adhesion and signaling on polymer substrates. *Journal of Biomedical Materials Research Part A* **2003,** *64* (1), 20-37. DOI: https://doi.org/10.1002/jbm.a.10316.
64. Gomes, R. R., Jr.; Farach-Carson, M. C.; Carson, D. D., Perlecan functions in chondrogenesis: insights from in vitro and in vivo models. *Cells Tissues Organs* **2004,** *176* (1-3), 79-86. DOI: https://doi.org/10.1159/000075029.
65. Robinson, D. E.; Marson, A.; Short, R. D.; Buttle, D. J.; Day, A. J.; Parry, K. L.; Wiles, M.; Highfield, P.; Mistry, A.; Whittle, J. D., Surface gradient of functional heparin. *Advanced Materials* **2008,** *20*, 1166-1169. DOI: https://doi.org/10.1002/adma.200702586.
66. Glennon-Alty, L.; Williams, R.; Dixon, S.; Murray, P., Induction of mesenchymal stem cell chondrogenesis by polyacrylate substrates. *Acta Biomater.* **2012**. DOI: https://doi.org/10.1016/j.actbio.2012.12.007.
67. Murphy, W. L.; McDevitt, T. C.; Engler, A. J., Materials as stem cell regulators. *Nat. Mater.* **2014,** *13* (6), 547-557. DOI: https://doi.org/10.1038/nmat3937.
68. O'Neill, J. D.; Freytes, D. O.; Anandappa, A. J.; Oliver, J. A.; Vunjak-Novakovic, G. V., The regulation of growth and metabolism of kidney stem cells with regional specificity using extracellular matrix derived from kidney. *Biomaterials* **2013,** *34* (38), 9830-9841. DOI: https://doi.org/10.1016/j.biomaterials.2013.09.022.

69. Kim, D. H.; Provenzano, P. P.; Smith, C. L.; Levchenko, A., Matrix nanotopography as a regulator of cell function. *J. Cell Biol.* **2012,** *197* (3), 351-60. DOI: https://doi.org/10.1083/jcb.201108062.
70. Ross, A. M.; Jiang, Z.; Bastmeyer, M.; Lahann, J., Physical aspects of cell culture substrates: topography, roughness, and elasticity. *Small* **2012,** *8* (3), 336-355. DOI: https://doi.org/10.1002/smll.201100934.
71. Dalby, M. J.; Gadegaard, N.; Tare, R.; Andar, A.; Riehle, M. O.; Herzyk, P.; Wilkinson, C. D. W.; Oreffo, R. O. C., The control of human mesenchymal cell differentiation using nanoscale symmetry and disorder. *Nat. Mater.* **2007,** *6* (12), 997-1003. DOI: https://doi.org/10.1038/nmat2013.
72. Dalby, M. J.; McCloy, D.; Robertson, M.; Wilkinson, C. D. W.; Oreffo, R. O. C., Osteoprogenitor response to defined topographies with nanoscale depths. *Biomaterials* **2006,** *27* (8), 1306-1315. DOI: https://doi.org/10.1016/j.biomaterials.2005.08.028.
73. McNamara, L. E.; McMurray, R. J.; Biggs, M. J. P.; Kantawong, F.; Oreffo, R. O. C.; Dalby, M. J., Nanotopographical control of stem cell differentiation. *Journal of Tissue Engineering* **2010,** *1* (1). DOI: https://doi.org/10.4061/2010/120623.
74. Curran, J. M.; Chen, R.; Hunt, J. A., The guidance of human mesenchymal stem cell differentiation in vitro by controlled modifications to the cell substrate. *Biomaterials* **2006,** *27* (27), 4783-4793. DOI: https://doi.org/10.1016/j.biomaterials.2006.05.001.
75. Holst, J.; Watson, S.; Lord, M. S.; Eamegdool, S. S.; Bax, D. V.; Nivison-Smith, L. B.; Kondyurin, A.; Ma, L.; Oberhauser, A. F.; Weiss, A. S., Substrate elasticity provides mechanical signals for the expansion of hemopoietic stem and progenitor cells. *Nat. Biotechnol.* **2010,** *28* (10), 1123-1128. DOI: https://doi.org/10.1038/nbt.1687.
76. Williams, D. F., On the mechanisms of biocompatibility. *Biomaterials* **2008,** *29* (20), 2941-2953. DOI: https://doi.org/10.1016/j.biomaterials.2008.04.023.
77. Zheng, W.; Zhang, W.; Jiang, X., Precise control of cell adhesion by combination of surface chemistry and soft lithography. *Advanced Healthcare Materials* **2013,** *2* (1), 2192-2640. DOI: https://doi.org/10.1002/adhm.201200104.

Figure captions

Figure 1: Surface chemical analyses. Oxygen/Carbon (O/C, black) and Nitrogen/Carbon (N/C, green) atomic ratio of (A) homo- and copolymers and (B) across the gradient. (C) Homo-and copolymer surface primary amine quantification using Coomassie Blue (CBB) method and (D) Orange 2 method. (E) Correlation between CBB and Orange 2 method. (F) Correlation between XPS ratio (N/C) and primary amine group density quantification obtained by colorimetry using CBB (blue) and Orange 2 (orange) method. The x-axis error bars correspond to the general XPS 10% error. Data represent an average of a minimum of 5 samples ± SD. Asterisks indicate statistical significance between substrates ($p<0.05$).

Figure 2: Sessile drop water contact angle of (A) AA and OD homo- and copolymers and (B) across the gradient. Date represent the mean of a minimum of 5 samples ± SD. (C) 2D water contact angle maps, representing the homogeneity of (sessile drop) contact angles across the surface plasma polymer coating. (D) Captive bubble contact angles 2 h post incubation of AA and OD homo- and copolymers in water (ddH_20, black) and FBS (grey). Error bars represent the standard error of a

minimum of 5 samples ±SD. Asterisks indicate statistical significance between substrates compared to a glass control (Tukey test, $p < 0.005$). (E) Protein adsorption BCA assay on 100%AA and 100%OD surfaces and tissue culture plate control (TCP) Error bars represent the standard error of a minimum of 5 samples ±SD. "!" symbol indicate statistical difference between TCP and OD, "#" between AA and TCP, "*" between AA and OD ($P < 0.05$)

Figure 3: mKSC morphology. Representative phase contrast and phalloidin/DAPI stained fluorescent images of mKSCs cultured on gradients (A) and homo- and copolymers (B) for 96 h. mKSCs were seeded at a density of 1 x 10^3 cells / well. White arrows indicate cells with podocyte-like morphology. Scale bar is 100 µm.

Figure 4: Differentiation of mKSCs into podocyte-like cells. There is a significant increase in the number of podocyte-like cells on amine-rich substrates. mKSCs were seeded at a density of 1 x 10^3 cells / well. (A) Quantification of podocyte-like cells on homo- and copolymers (black bars) and gradients (green bars). (B) Correlation of the amount of podocyte-like cells 96h post seeding with surface amine content as quantified using XPS ratio (N/C) analysis on homo-and copolymers (black) as well as gradients (green), respectively. Asterisks indicate significant differences compared with glass control ($p < 0.05$, Tukey test). Results represent the mean of three biological replicates. (C) Nephrin staining of mKSCs cultured on homo- and copolymers and (D) Nephrin staining of mKSCs cultured on gradients. Blue: DAPI. Red: Nephrin. White arrows indicate binuclear podocyte-like cells. Scale bar: 100 µm.

Figure 5: Differentiation of mKSCs into PTCs. There is a significant increase in the number of PTC-like cells on methyl-rich substrates. mKSCs were seeded at a density of 1 x 103 cells / well and cultured for 96 h. (A) Megalin staining of mKSCs cultured on gradient substrates and (B) on homo- and copolymers. Blue: DAPI. Red: megalin. Scale bar: 100 µm (C) Quantification of megalin expressing cells on gradients and (D) homo- and copolymers at three time points, 6 h, 48 h and 96 h post seeding. (E) Flow cytometry data showing F-BSA uptake of cells cultured for 96 h on homo and copolymers. (F) Quantification of F-BSA+ cells cultured on homo- and copolymers. Asterisks indicate significant difference compared to a glass control ($p < 0.05$, Tukey test). Results represent the mean of three biological replicates. (G) Alkaline Phosphatase staining of mKSCs cultured on heteropolymers and AA/OD rich sections of the gradient substrates compared to a glass control. Scale bar: 100 µm